Astron. Astrophys. 355, 1087–1097 (2000)

ASTRONOMY AND ASTROPHYSICS

Distribution of starspots on cool stars

II. Pre-main-sequence and ZAMS stars between 0.4 $M_\odot$ and 1.7 $M_\odot$

Th. Granzer[1], **M. Schüssler**[2], **P. Caligari**[2], **and K.G. Strassmeier**[1]

[1] Institut für Astronomie, Universität Wien, Türkenschanzstrasse 17, 1180 Vienna, Austria (granzer,strassmeier@astro.univie.ac.at)
[2] Kiepenheuer Institut für Sonnenphysik, Schöneckstrasse 6, 79104 Freiburg, Germany (msch,cale@kis.uni-freiburg.de)

Received 15 June 1999 / Accepted 27 September 1999

Abstract. We study the dynamics of magnetic flux tubes in young stars with masses between 0.4 $M_\odot$ and 1.7 $M_\odot$ and for rotation rates between 0.25 $\Omega_\odot$ and 63 $\Omega_\odot$. The resulting latitudinal emergence patterns at the stellar surface are compared with observed distributions of starspots in stellar latitude. The stellar models considered cover the range of evolutionary stages from shortly after the Hayashi phase down to the ZAMS, i.e. from the classical and weak-line T Tauri stars to the α-Persei stars. We use numerical simulations to follow the evolution of magnetic flux tubes from their origin at the bottom of the convection zone up to near-surface layers. We find a strong increase of emergence latitude with increasing rotation rate, a moderate decrease with increasing stellar mass, and a stronger decrease with stellar age. At very early evolutionary stages, when the central radiative zone is still quite small, we find magnetic flux emergence both in low latitudes as well as in the polar areas. High-latitude emergence is predicted in slightly more evolved pre-main-sequence and young main-sequence stars, but truly polar spots on these stars require an additional transport mechanism acting after magnetic flux emergence at the surface, probably meridional circulation or poleward slip of the 'anchored' part of the erupted flux tubes. We discuss our findings in the light of the results obtained from Doppler-imaging studies.

Key words: Magnetohydrodynamics (MHD) – stars: rotation – stars: pre-main sequence – stars: magnetic fields – stars: activity

1. Introduction

Doppler-imaging techniques reveal cool spots on the surfaces of rapidly rotating, magnetically active stars. Spots are found predominantly at high stellar latitude, often straddling the poles (Vogt & Penrod 1983; for a recent summary see Vogt et al. 1999). These results are in striking contrast to the solar case, for which spots occur only within about $\pm 30^\circ$ of the equator. After some debate concerning the reliability of the Doppler-imaging technique (e.g. Byrne 1996, Unruh & Collier Cameron 1997, Hatzes et al. 1996, Bruls et al. 1998), the reality of the polar spots now seems to be established.

Send offprint requests to: Th. Granzer

Schüssler & Solanki (1992) suggested that rapid stellar rotation is responsible for the appearance of polar magnetic features. They showed that the Coriolis force leads to strong poleward deflection of a magnetic flux tube rising through the convection zone of a rapidly rotating cool star. A first detailed study of flux-tube dynamics in stars other than the Sun was presented by Schüssler et al. (1996, hereafter Paper I; see also Schüssler 1996). They followed the approach of Caligari et al. (1995), which successfully reproduces many observed properties of sunspot groups: flux tubes stored in a layer of overshooting convective motion at the bottom of the convection zone are amplified by differential rotation until the Parker instability sets in once a critical field strength is exceeded. As a consequence, flux loops rise toward the surface and form sunspots and active regions upon emergence. The extension of this approach to rapidly-rotating stars carried out in Paper I confirmed the validity of the estimates of Schüssler & Solanki (1992). Similar results were found by DeLuca et al. (1997). While these studies considered only stars of one solar mass, the growing number of Doppler-imaging observations of a variety of stars requires models covering a larger range of stellar masses. Therefore, we have calculated stellar models with masses between 0.4 $M_\odot$ and 1.7 $M_\odot$ and carried out flux-tube simulations for these models assuming a wide range of rotation rates.

In Sect. 2, we present the stellar models and compare them with previously computed models. The basic properties of the magnetic flux tubes are discussed in Sect. 3. In Sects. 4 and 5, we present the results of the simulations and discuss the spot emergence patterns in dependence of stellar rotation rate, evolutionary stage, stellar mass, and flux tube parameters. In Sect. 6, we discuss the results and compare them with observational findings from Doppler imaging. Our conclusions are given in Sect. 7.

2. Stellar models

The stellar models were calculated with an updated version of the Kippenhahn et al. (1967) stellar evolution code. To account for the low temperatures and high densities during the pre-main-sequence evolution, we used opacities of Alexander & Ferguson (1994) to complement the OPAL opacities (Iglesias & Rogers

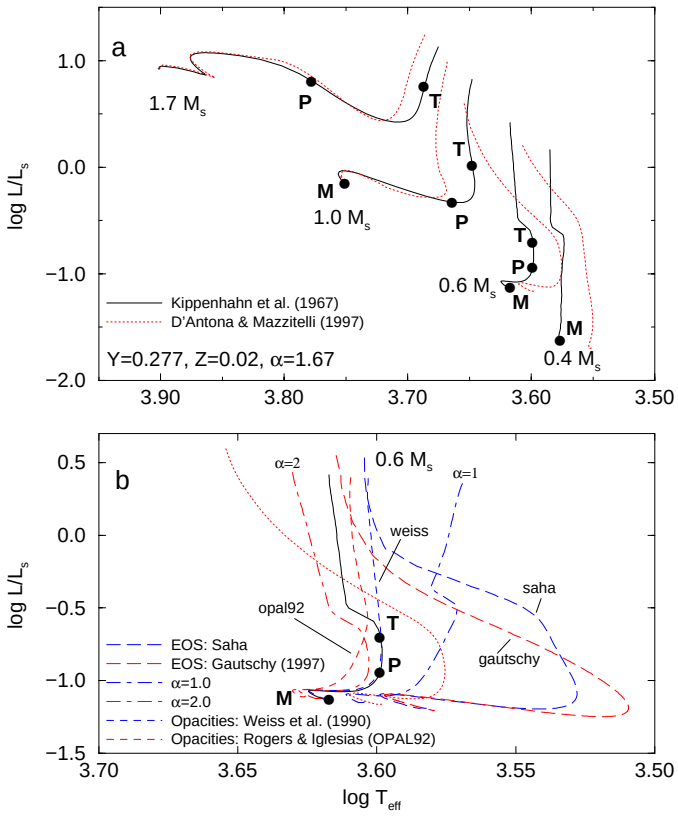

Fig. 1a and b. Theoretical HR diagrams. Panel **a** shows the pre-main-sequence tracks for 0.4, 0.6, 1.0, and 1.7 $M_\odot$ (solid lines) and indicates the evolutionary stage of the adopted models (M, P, and T). For comparison, we also show tracks (dotted lines) calculated by D'Antona & Mazzitelli (1997). Panel **b** is a close-up of evolutionary tracks for the 0.6-$M_\odot$ model based upon different opacity tables, equations of state (EOS), and mixing-length parameter α.

1996) at the low-T/high-ρ end. The OPAL equation of state (Rogers et al. 1996) was used whenever applicable, otherwise the MHD equation of state (Mihalas et al. 1990) was adopted. Local mixing-length theory was used for modeling the convection zone. Comparing a model of a 1-$M_\odot$ star at an age of 4.6 Gyr with the present Sun confines the mixing-length parameter to $\alpha = 1.67$ and the initial helium abundance to $Y = 0.277$. Metallicity in all models was set to $Z = 0.02$.

Fig. 1a shows a theoretical HR diagram giving the evolutionary tracks resulting from our computations. The particular stellar models adopted for flux-tube simulations are indicated. For comparison, tracks computed by D'Antona & Mazzitelli (1997) are also shown (dotted lines). The rather large discrepancy for the low-mass models is due to increasing uncertainties in the opacities and equations of state (EOS). To better estimate the impact of these uncertainties, we carried out test calculations as summarized in Fig. 1b. We used a strictly Saha-type EOS as well as a 'Saha-like' EOS from Gautschy (priv. comm.), two alternative sets of opacities from OPAL92 (Rogers & Iglesias 1992) and from Weiss et al. (1990), respectively, and we also varied the mixing-length parameter, α, from 1.0 to 2.0. The influence of these variations on the flux-tube simulation results is quite small (see Sect. 5.4, Table 3).

Table 1. Parameters of stellar models

Stage	$M/M_\odot$	Age/10^6yr	$L/L_\odot$	$R/R_\odot$	$T_{\rm eff}$/K
T	0.6	8.3	0.20	0.95	3970
T	1.0	2.4	1.06	1.74	4440
T	1.7	0.55	5.75	3.39	4860
P	0.6	21.1	0.12	0.71	3970
P	1.0	14.3	0.47	1.08	4610
P	1.7	7.4	6.44	2.36	5990
M	0.4	1500	0.024	0.37	3770
M	0.6	520	0.075	0.53	4140
M	1.0	140	0.72	0.89	5630

The selection of stellar models for the flux-tube simulations is guided by the necessity of an overshoot layer for flux tube storage, i.e. the models must exhibit a radiative zone below an outer convective layer. On the zero-age main sequence (ZAMS) such a configuration is found in the mass range between about 0.4 $M_\odot$ and 1.5 $M_\odot$. Pre-main-sequence (PMS) stars with masses larger than 1.5 $M_\odot$ also have a core-envelope structure during their descent from the Hayashi line. We therefore adopted a 1.7 $M_\odot$ stellar model as the high-mass end for the early evolutionary stages. Arriving at the ZAMS, the 1.7 $M_\odot$ has become entirely radiative and can no longer be considered within the framework of our flux-tube model. Instead, we have added a model with 0.4 $M_\odot$ to our ZAMS selection. The results of flux-tube simulations for the PMS phases of this model are very similar to those of the 0.6 $M_\odot$ model, so that there is no need to discuss them further. In summary, we have performed flux-tube simulations for ZAMS stars with masses of 0.4 $M_\odot$, 0.6 $M_\odot$, and 1.0 $M_\odot$ and for PMS stars with 0.6 $M_\odot$, 1.0 $M_\odot$, and 1.7 $M_\odot$. We have chosen stellar models in three distinct evolutionary stages (labeled T, P, and M in Fig. 1), defined in the following way:

- T, the T-Tauri stars, confine 5% of their mass in the radiative core;
- P, the PMS stars, generate 1% of their entire luminosity by nuclear reactions;
- M, the ZAMS stars, show a central depletion of 1% of their initial hydrogen content.

Table 1 summarizes the properties of the models selected for the flux-tube simulations. We have determined the overshoot layer for these models following the precepts of Shaviv & Salpeter (1973) and Skaley & Stix (1991). Table 2 lists the parameters of the resulting overshoot layers. Recent helioseismic data (Basu & Antia 1997, Basu 1997) suggest a smaller thickness of the solar overshoot layer than what we use here. However, these estimates are based upon the assumption of strictly spherically symmetric and time-independent overshoot, which may not necessarily be adequate for the real Sun or other stars. Even if the stellar overshoot layers would be somewhat thinner than the values given in Table 2, this would mainly affect the total amount of flux that can be stored, but not so much the

Table 2. Structure of the overshoot layer. $R_\star$: stellar radius in Mm, $r_{\rm bot}$: bottom radius; Δr: thickness (given in Mm and as a fraction of the local pressure scale height); r_δ: radius, where $\delta \equiv \nabla - \nabla_{\rm ad} = 0$. The last column gives the value of δ at the adopted equilibrium position, r_0, of the flux tube (2000 km above the bottom of the overshoot layer).

Model	$R_\star$	$r_{\rm bot}$	Δr		r_δ	$\delta(r_0)$
	(Mm)	(Mm)	(Mm)	(H_p)	(Mm)	(10^{-6})
T 0.6	660	56	106	0.24	283	–1.2
T 1.0	1210	83	213	0.22	521	–11.
T 1.7	2360	223	362	0.25	1020	–96.
P 0.6	494	190	28	0.29	271	–0.23
P 1.0	734	409	26	0.29	487	–12.
P 1.7	1640	1270	30	0.27	1360	–200
M 0.4	255	96	16	0.30	141	–0.017
M 0.6	371	224	12	0.29	257	–0.12
M 1.0	498	435	15	0.29	478	–2.99

emergence paths of individual flux tubes that are our primary concern here.

3. Model assumptions

The computations start with thin magnetic flux tubes stored in mechanical equilibrium in the overshoot layer below the stellar convective envelope. Small disturbances trigger the undulatory (Parker) instability and the simulation follows its nonlinear development close to the stellar surface, where the thin flux-tube approximation breaks down. The drag of the surrounding plasma on the rising tube is modeled by an aerodynamic drag term. We assume adiabatic thermal evolution of the flux tubes since the time scale for radiative energy exchange is much longer than the rise time of an unstable flux tube (Moreno-Insertis 1983). The code used to perform the simulations has been described by Caligari et al. (1995). In the following subsections, we explain how the initial state of the flux tubes is determined and argue to justify further model assumptions.

3.1. Critical field strength

As discussed in detail in Paper I, the initial field strength of the flux tubes is chosen according to a linear stability analysis (Ferriz-Mas & Schüssler 1993, 1995), assuming a growth time for the Parker instability of 300 days. The resulting 'critical' field strengths as a function of stellar latitude for various rotation rates between 0.25 and 63 $\Omega_\odot$ are given in Fig. 2. The different azimuthal wave numbers m of the most unstable mode are visible as the different line styles. The following conclusions can be drawn from Fig. 2:

- Flux tubes with a field strength below 10 T are stable.
- The critical field strength increases with Ω and decreases with stellar age.
- $m = 0$ (axisymmetric) modes are only present at very high latitudes or in very young stars.
- $m = 1$ is the dominant mode for all but the T models.
- $m = 2$ can intersect regions of $m = 1$ modes in the case of ZAMS stars with large rotation rate.
- $m = 3$ is found only in slowly-rotating, young stars with extremely small cores.

3.2. Magnetic flux

The magnetic flux carried by a flux tube is determined by its field strength and its diameter. The latter must be significantly smaller than the thickness of the overshoot layer corresponding to the assumption of isolated flux tubes. We consider flux tubes with a magnetic flux of 10^{14} Wb (10^{22} Mx), similar to typical fluxes for large solar active regions. In the thin-flux-tube approximation, the magnetic flux enters the equation of motion only via the flux tube diameter, which determines the influence of the aerodynamic drag force. The flux value assumed for our calculation yields already flux tube diameters sufficient for the drag force to be almost negligible in most cases, so that our simulation results and emergence patterns are also relevant for larger fluxes. In fact, the observed spot areas on active stars are significantly larger than those on the Sun. This could either mean that there are tubes with much larger magnetic fluxes than in the solar case or that the spot area results from a large number of emergences of smaller tubes, similar to the persistent 'active nests' on the Sun (e.g., Zwaan 1987). Both possibilities are thus in principle covered by our simulations (cf. Sect. 5.2).

3.3. Internal rotation profile

Helioseismic measurements (e.g. Schou et al. 1994, Tomczyck et al. 1995, Corbard et al. 1997, Charbonneau et al. 1998) show that the latitude-dependent differential rotation at the solar surface prevails throughout the convection zone. The radiative core is rotating almost rigidly, leading to a shear layer ('tachocline') at the bottom of the convection zone. For the solar case, Caligari et al. (1995) found that the stability criteria and the dynamics of rising flux tubes are not significantly affected by (radial and latitudinal) differential rotation. Observations of rapidly rotating spotted stars indicate much lower differential surface rotation than on the Sun (Hall 1990, Johns-Krull 1996). This is in agreement with theoretical models (Kitchatinov & Rüdiger 1995, Küker & Rüdiger 1997), which predict almost rigidly rotating convection zones for fast rotators. This does not exclude the existence of a radial shear layer between core and envelope as in the case of the Sun; in fact, such a layer is probably essential for the generation of toroidal magnetic field and flux tubes in the first place. In this paper, we do not address the amplification of magnetic field but only its evolution once a flux tube has formed and has become unstable. In this context, the reported amount of differential rotation has no significant influence and we thus adopt rigid rotation.

3.4. The stellar-surface limit

Close to the stellar surface, the thin flux-tube approximation utilized in the simulation code is violated because the tube di-

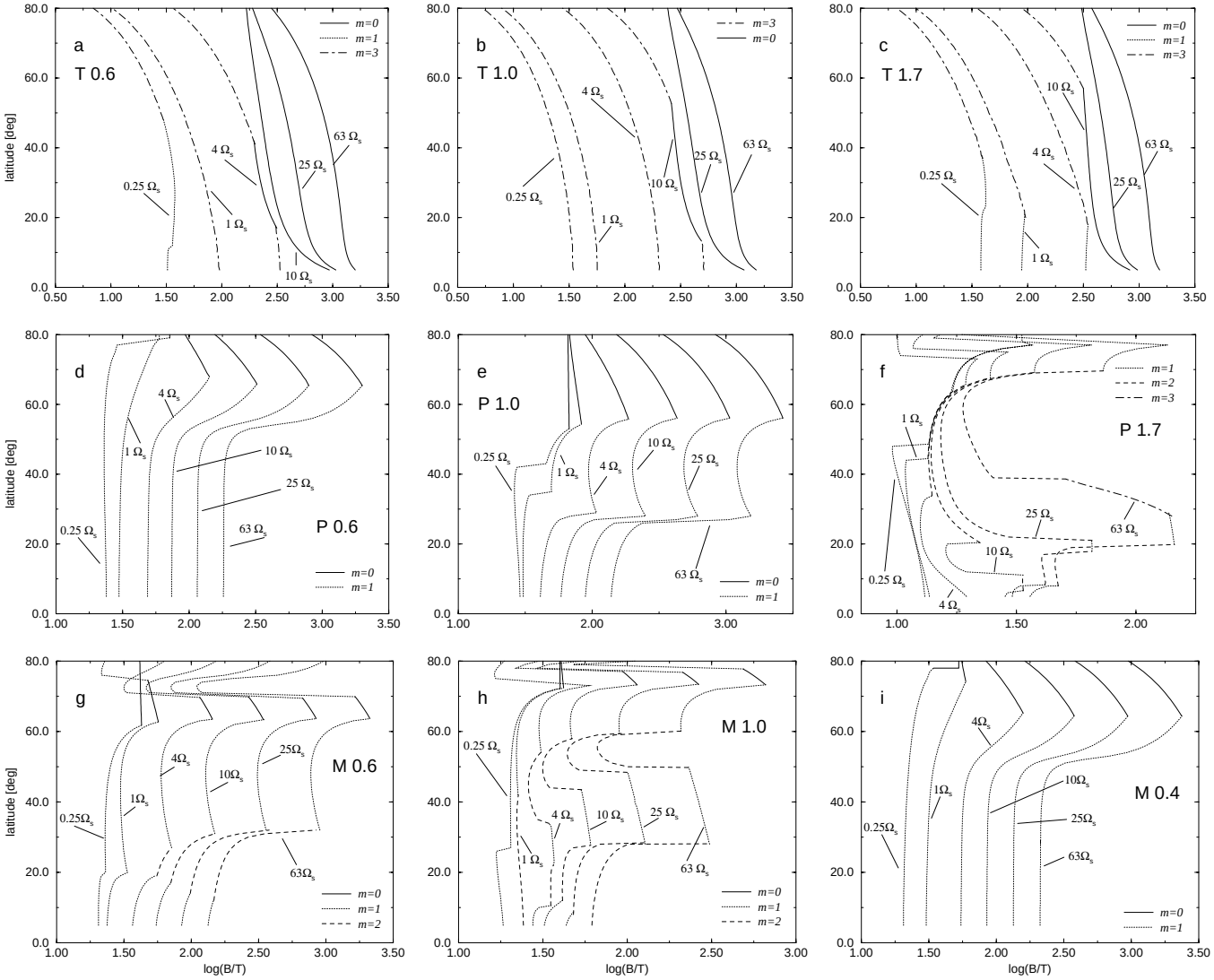

Fig. 2a–i. Critical field strengths (corresponding to 300 days growth time of the Parker instability) as a function of latitude for various rotation rates. Panels **a**–**c** (top row) show the T-Tauri models, panels **d**–**f** (middle row) show the PMS models, and panels **g**–**i** (bottom row) show the ZAMS models. The line styles indicate the azimuthal wave number m of the most unstable mode.

ameter becomes larger than the local pressure scale height. Our calculations are terminated at that point. Nevertheless, we can trace the development of a flux tube up to about 98% of the stellar radius. A radial extrapolation of the tube apex up to the stellar photosphere is then used to define the emergence latitude. There is no reason why the tube should suffer a significant deflection in latitude during its rise through the last 2% of the stellar radius. On the other hand, we cannot follow any latitudinal migration of the bipolar magnetic region (due to, e.g., meridional flow) after its emergence.

4. Patterns of flux emergence: the 'standard' cases

Schüssler & Solanki (1992) pointed out that the emergence latitude of a flux tube depends on the interplay between the buoyancy force and the Coriolis force. A dominant Coriolis force constrains the flux tube to a rise parallel to the axis of rotation, leading to flux emergence at a stellar latitude that is determined by the relative size of the radiative core. Consequently, for rapidly rotating stars with a small core, magnetic flux emerges close to the stellar poles.

For each of the stellar models from Table 1, we have simulated the evolution of linearly unstable flux tubes with equilibrium latitudes between 5° and 60° (12 tubes in steps of 5°). The stellar rotation rates assumed are 0.25, 1, 4, 10, 25, and 63 $\Omega_\odot$. The results show that, depending on the radius of the core, the rise of the flux tubes through the convective envelope follows two rather distinct scenarios (Fig. 3):

1) As long as the radiative core is not too small, we find a similar evolution of the unstable flux tubes as in Paper I (see Fig. 3a, here for $m = 1$). Non-axisymmetric instability ($m > 0$) starts with the formation of m crests and troughs. Gravity leads to a downflow of matter from the crests to the troughs which in-

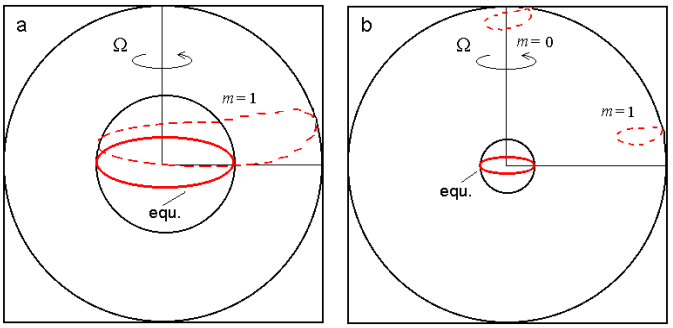

Fig. 3a and b. Schematic illustration of the evolution of unstable flux tubes in stars with large (panel **a**) and small (panel **b**) radiative cores. The tubes evolve from their initial toroidal equilibrium state (marked 'equ.') into the configurations indicated by dashed lines. For large and intermediate core sizes (P- and M-models), the main part of the flux tube remains anchored in the overshoot layer. For small cores (T-models), the entire tube becomes disconnected from the overshoot region and floats to the surface in the form of a closed loop. It emerges either near the pole ($m = 0$) or at low latitudes ($m \geq 1$).

creases the buoyancy of the crests upwards, while the troughs continue to sink toward the bottom of the overshoot layer. Typically, one of the crests evolves more rapidly than the others; after it enters the superadiabatic part of the convection zone, it rapidly crosses the convective envelope and emerges at the surface. During this rise, the lower 'anchored' part of the flux tube moves slowly poleward along the bottom of the overshoot layer because the rise of the loop has offset the flow along the tube balancing the magnetic curvature force in mechanical equilibrium (Moreno-Insertis et al. 1992). This sequence of events applies to all M- and P-models.

2) If the radiative core is very small (as in the case of the T-models), the curvature force dominates and the poleward slip of the anchored part of the flux tube becomes faster than the buoyant rise of the crest. As a result, the bottom part of the tube actually passes through the rotation axis toward the other side of the star, where the combined action of crest buoyancy and curvature force on the bottom detach the entire tube from the overshoot layer and leave it floating freely in the convection zone. In this situation, the resulting force from the radially inward directed (negative) buoyancy of the trough and the outward buoyancy of the crest has a component directed toward the equator, so that emergence takes place in low to middle latitudes (see Fig. 3b, case $m = 1$). Flux tubes in all slowly-rotating ($\Omega \lesssim 10\ \Omega_\odot$) T-models follow this pattern. In the case of rapidly rotating T-models, axisymmetric instability ($m = 0$) dominates and the flux tubes (in this case, flux rings) rise parallel to the rotational axis to emerge close to the stellar pole (Fig. 3b, case $m = 0$). In some cases, if the field strength is sufficiently large, the flux ring shrinks so much under the influence of the curvature force that it completely loses buoyancy in the middle of the convection zone and stops to rise. An example can be seen in Fig. 5 (right panel), where the path of the flux tube that starts at $60°$ ends within the convection zone. The fate of these flux rings is unclear. We may speculate that continuous gnawing and transport by convective flow together with radiative heating eventually would bring the magnetic flux to the surface, albeit probably in a fragmented, incoherent form.

4.1. Dependence on rotation rate and evolutionary state

From the twelve emergence latitudes of flux tubes resulting for each stellar model and each rotation rate, we have derived a 'spot probability function' (SPF) by calculating, for any given latitude, the reciprocal of the average latitude difference to the twelve emergence points. The SPF reflects the expected distribution of stellar spots in latitude for the case of a uniform release of flux loops from the overshoot region below $60°$ latitude.

Fig. 4 shows the spot probability function for all models as a function of the stellar rotation rate. For the ZAMS models, a 0.4-$M_\odot$ model is shown instead of the fully radiative 1.7 $M_\odot$ star. A striking feature of Fig. 4 is the increasing probability of high-latitude spots with faster rotation in case of the PMS and ZAMS stars. This is due to the fact that the Coriolis force increases more rapidly with rotation rate than the critical field strength, which determines the buoyancy force. On the other hand, the T-Tauri stars (upper panel of Fig. 4) behave differently. Between 1 and 10 $\Omega_\odot$, the emergence latitude stays roughly constant or even decreases slightly, while above 10 $\Omega_\odot$ the flux tubes emerge predominantly near the pole. The reason for this behaviour lies in the evolution scheme for the flux tubes in the T-stars described above. For rotational rates $\Omega \lesssim 10\ \Omega_\odot$, the dominant mode of flux tube instability is non-axisymmetric, i.e. $m \geq 1$. The flux tubes cross the pole and are deflected toward the equator. This deflection is caused by the buoyancy force and does not strongly depend on the rotation rate. The emergence latitude is therefore more or less independent of the rotation rate as long as the $m \geq 1$ modes dominate. For $\Omega \gtrsim 10\ \Omega_\odot$, the preferred mode of instability is the axisymmetric ($m = 0$) mode with eruption in the polar regions. However, some of the originally m=0-unstable tubes, mainly those starting at low latitudes, develop a secondary $m = 1$ instability before they leave the overshoot layer. These flux tubes evolve similar to the 'normal' $m = 1$ tubes: they cross the pole and are deflected toward the equator. This leads to a complete separation of the active regions of these stars, a polar cap accompanied with some spots at low to medium latitudes. All T models with rotation rates above 10 $\Omega_\odot$ follow this pattern.

Another key result from Fig. 4 is the decrease of emergence latitude with increased stellar mass and age. Both dependencies are caused by the growing size of the radiative core. For purely geometric reasons, a rise parallel to the axis of rotation then leads to decreasing emergence latitudes. Furthermore, the ratio of the rise time through the less extended convective envelope to the inertial frequency, 2Ω, becomes smaller, leading to less significant poleward deflection (Schüssler 1996, see also Buzasi 1997). Geometry is also responsible for the 'saturation' of the emergence latitudes for the PMS and ZAMS stars in case of sufficiently large rotation rates ($\Omega \gtrsim 10\ \Omega_\odot$). Once the rotation is fast enough to force the flux tubes to rise parallel to the axis, further increase of the rotation rate no longer significantly af-

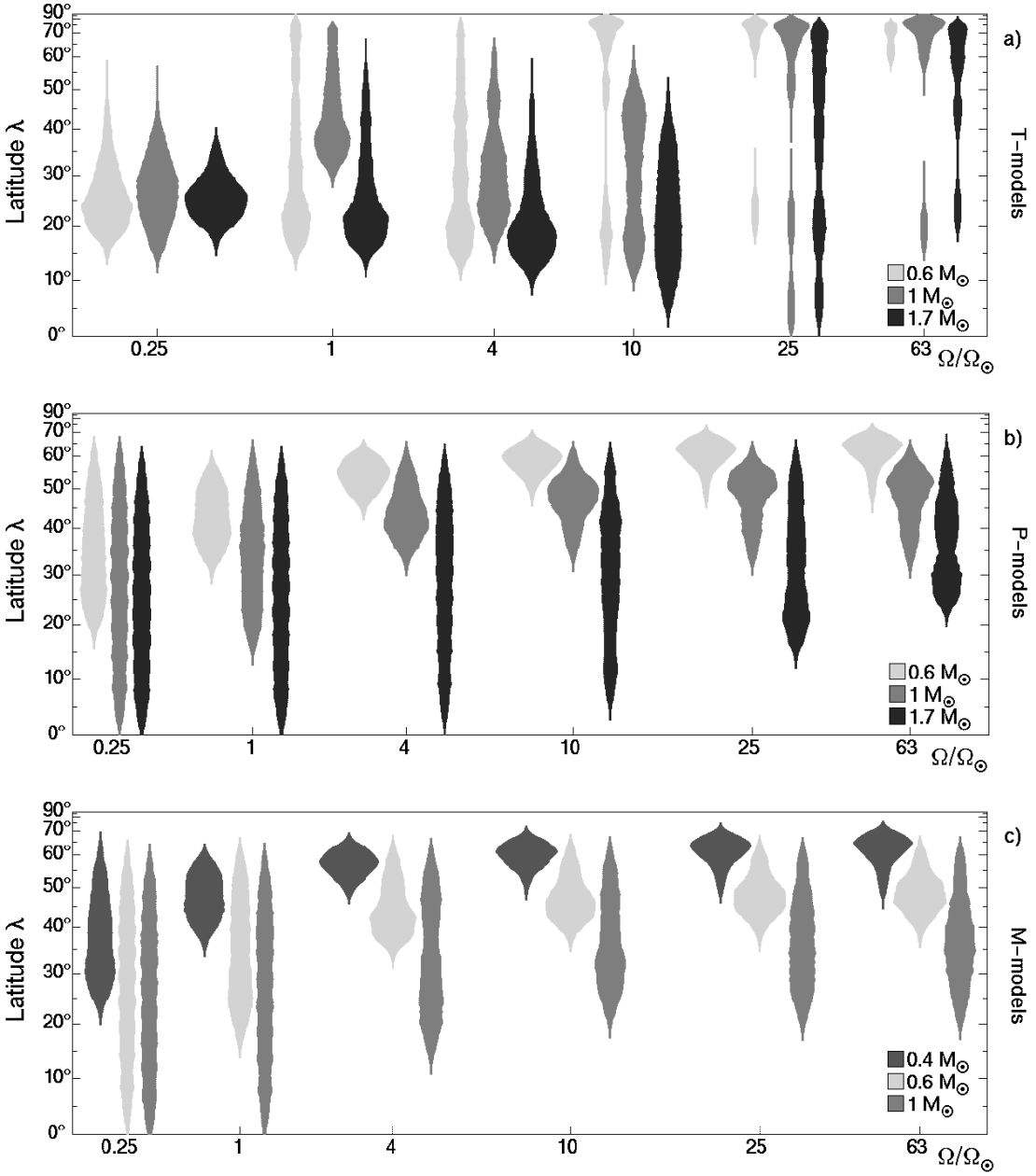

Fig. 4a–c. Spot probability function (SPF) versus stellar rotation rate. Each vertical strip represents a stellar model. Its width at any given latitude is proportional to the value of the SPF. The top panel **a** is for T-Tauri stars (T models in Fig. 1), the middle panel **b** for PMS stars (P models), and the bottom panel **c** is for the ZAMS stars (M models; the 1.7 $M_\odot$ model is replaced by a model with 0.4 $M_\odot$). Note the 'saturation' of emergence latitudes for $\Omega \gtrsim 4\ \Omega_\odot$ in the case of the lower-mass PMS and ZAMS models. The ordinate scale is proportional to $\sin\lambda$ in order to represent the corresponding spherical surface area.

fects the emergence latitude. Since models P0.6 and M0.4 have the smallest cores of the P- and M-models, rotational effects are most pronounced. These models show saturation already at relative low rotation rates. Note that the emergence patterns for models P0.6 and M0.4 are almost identical. This results from the nearly equal size of their radiative cores (0.38 $R_\star$) together with the similar values of the critical field strengths (cf. Fig. 2d and 2i).

As mentioned before, in the case of a dominant $m = 0$ instability together with rapid stellar rotation, a flux tube may be prevented from reaching the stellar surface due to a loss of buoyancy. This affects particularly the T0.6 model, for which most of the tubes do not erupt, leading to small values of the SPF in the top panel of Fig. 4.

5. Parameter study

In order to explore the sensitivity of our results to some of the model assumptions, we have varied some of the parameters of our standard cases. For each test calculation, we determine a

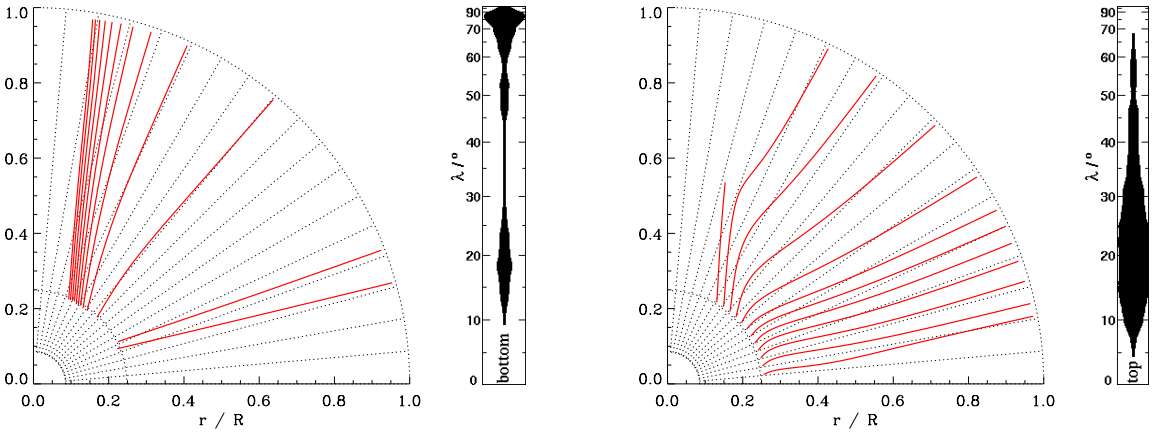

Fig. 5. Paths of flux-loop summits for model T0.6 with $\Omega = 10\ \Omega_\odot$. Left panel: initial location 2000 km above the bottom of the overshoot region ($\simeq 0.1R$). Right panel: initial location 2000 km below the upper boundary of the overshoot layer ($\simeq 0.25R$). Starting latitudes in both cases are between 5° and 60°. Note that the paths (thick lines) are only shown after the summit has entered the convection zone; the parts within the overshoot layer are omitted for clarity. The small panels are the corresponding SPFs.

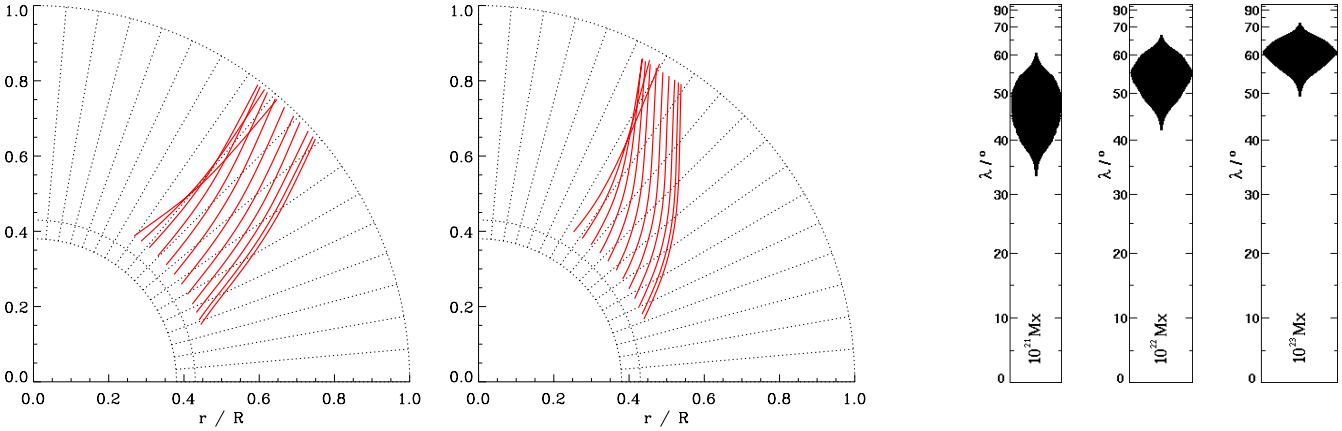

Fig. 6. Dependence of the summit paths on magnetic flux for model P0.6 with $4\,\Omega_\odot$. The left two panels show the paths of rising flux loops with a total magnetic flux of 10^{21} Mx (left) and 10^{23} Mx (middle). The three panels to the right give the spot probability function for 10^{21}, 10^{22}, and 10^{23} Mx, respectively.

latitude deviation parameter defined as $\epsilon \equiv \lambda_{\rm test} - \lambda_{\rm std}$, where $\lambda_{\rm std}$ and $\lambda_{\rm test}$ are the emergence latitudes for the standard parameter choice and for the test value, respectively.

The results are summarized in Table 3, arranged with respect to decreasing importance of the effect. The first column identifies the parameter or property that has been varied, the second column gives the stellar model, for which the largest deviation occurs. The remaining three columns in Table 3 indicate the effect on the emergence latitudes: $\epsilon_{\rm av}$ is the average of the absolute values of ϵ for all flux tubes (the sign of $\epsilon_{\rm av}$ indicates the sign of the majority of individual values), $\epsilon_{\rm max}$ is the maximum value of ϵ and $\lambda_{\rm start}$ is the initial latitude of the corresponding flux tube.[1]

[1] Parameter variations that influence stellar evolution lead also to changes of the luminosity and effective temperature of the star. For the very sensible case of a 0.6 $M_\odot$ star we give the different evolutionary tracks in Fig. 1b.

5.1. Initial location of the flux tube

In the standard cases, the equilibrium position of the flux tube is 2000 km above the bottom of the overshoot layer. To estimate the consequences of varying this assumption, we performed calculations for the other extreme, i.e. took the initial location of the tube as 2000 km below the top of the overshoot layer. The choice of the initial location affects the critical field strength mainly through the depth dependence of the subadiabaticity of the stratification in the overshoot layer. In stars with very small cores and thick overshoot layers (i.e. the T models) the radius of curvature, R, of the flux-tube ring may change by a factor of two. Because of the $1/R$-dependence of the magnetic tension it is much more pronounced in the standard case than in the test case. If we consider further that m=0-instability is always driven by a dominant magnetic tension, we can explain the T0.6 model with a rotation rate of $\Omega = 10\ \Omega_\odot$, where we found the largest value of $\epsilon_{\rm av}$. The dominant mode of the instability changes from

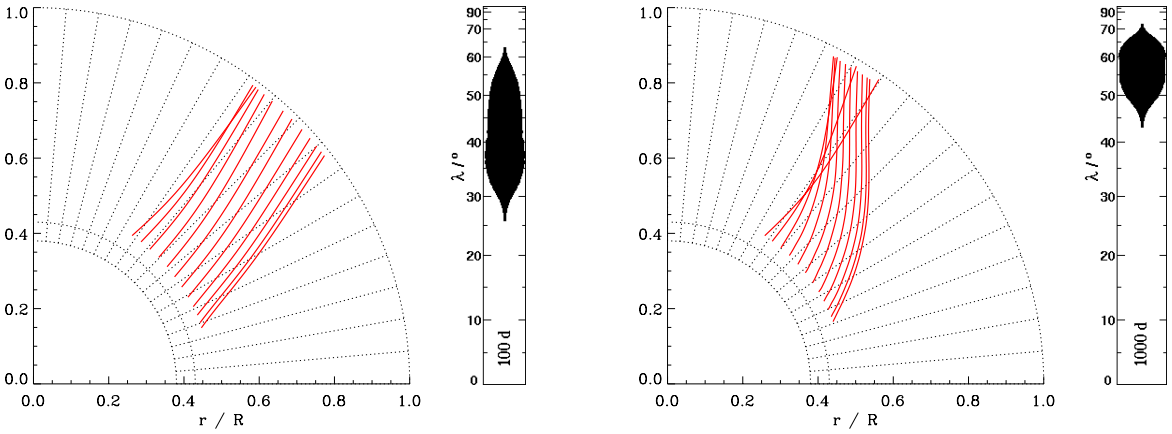

Fig. 7. Dependence of the summit paths on the growth time of the Parker instability for model P0.6 with $4\,\Omega_\odot$. Left: 100 days growth time; Right: 1000 days growth time.

Table 3. Maximum deviation of the emergence latitude from the standard cases. Given are the values for those models that show the largest effects.

Parameter	Model ($M_\odot$,$\Omega_\odot$)	$\epsilon_{\rm av}$ (°)	$\epsilon_{\rm max}$ (°)	$\lambda_{\rm start}$ (°)
Flux tube properties:				
Start. depth	T 0.6,10	–32.7	–49.5	30
Magnetic flux	P 0.6,4	+7.4	+8.8	5
Growth time	P 0.6,4	+6.8	+9.6	5
Stellar structure:				
Code	P 0.6,4	+3.1	+12.5	60
EOS	P 0.6,4	–1.7	–2.5	55
Opacity	P 0.6,4	+0.8	+1.4	60
Mixing length	P 0.6,4	+0.6	+0.8	50

$m = 0$ to $m = 3$ as we raise the initial location of the flux tube so that, as discussed above, the mainly polar emergence in the standard case changes gradually to flux emergence at low and middle latitudes. For both cases, Fig. 5 shows the paths of the flux-loop summits in a meridional cut through the star together with the corresponding SPFs. While the large size of the overshoot layer in the case of the T-models leads to significant variations of the parameters relevant for the stability between top and bottom of the overshoot layer, the changes are much less for the P- and M-models, for which $\epsilon_{\rm av}$ remains always below $5°$.

5.2. Amount of magnetic flux

Two cases with a total flux of 10^{21} and 10^{23} Mx were considered and compared to the standard case with 10^{22} Mx. Fig. 6 shows the paths of the flux-loop summits together with the corresponding SPFs for the most sensitive model, namely P0.6 with $4\,\Omega_\odot$. The magnetic flux affects the evolution of a flux tube through the drag force, which depends on the diameter of the tube. For constant field strength, decreasing flux increases the drag force and vice versa. The drag force affects both the rising speed of the flux tube and its exchange of angular momentum with the surrounding medium (for $m \neq 0$). Increasing angular-momentum transfer for decreasing magnetic flux diminishes the effect of the Coriolis force and, therefore, reduces the poleward deflection of rising flux loops (Choudhuri & D'Silva 1990, Fan et al. 1993). As a consequence, tubes with a larger amount of flux emerge at higher latitudes. However, Fig. 6 shows that the effect on the SPFs is not dramatic.

5.3. Growth time of the instability

We have changed the linear growth time of the Parker instability from its initial value of 300 days to the extreme values of 100 and 1000 days, respectively. Fig. 7 shows flux-loop trajectories and SPFs for the most strongly affected case (P0.6 with a rotation rate of $4\,\Omega_\odot$). Since the critical field strength depends markedly on the growth time in the case of the P-models, the initial field increases by a factor 2.5 when changing the growth time from 1000 to 100 days. The larger field strength leads to a stronger buoyancy force, causing a weaker poleward deflection for the case with a growth time of 100 days.

5.4. Stellar structure

The effect of changing the underlying stellar models has been tested using different EOS, opacities, mixing-length parameters and also by performing flux-tube simulations on the basis of a stellar model obtained from an independent source. Changes of the overall spot pattern were always below $5°$. Perhaps the most interesting case is the test with stellar models computed with an independent stellar-evolution code. To this end we used a 0.6-$M_\odot$ PMS model kindly provided by I. Mazzitelli (cf. D'Antona & Mazzitelli 1997). The maximum $\epsilon_{\rm av}$ found in this comparison amounts to only $3°$; this is smaller than the effects caused by variations of the initial state of the flux tubes.

Further tests with a different EOS (Gautschy priv. comm.), different opacities (Weiss et al. 1990) and different mixing-length parameters revealed even smaller effects, $\epsilon_{\rm av} \lesssim 1°$.

6. Comparison with observations and discussion

Our simulations show that rising flux tubes emerge at high stellar latitudes in the case of rapid rotation ($\Omega \gtrsim 10\ \Omega_\odot$). This is in general agreement with the abundant observations of high-latitude and polar spots on rapidly rotating active stars. Since the Coriolis force can at most lead to a rise parallel to the axis of rotation, the actual value of the emergence latitude depends on the relative size of the stellar radiative core. Consequently, we find truly polar emergence for models of very young (T-Tauri like) stars with small radiative cores. We suggest that on these stars the polar regions are filled up with starspots from the continuous emergence of m=0-unstable flux tubes, so that a cool and relative stable polar cap develops. On the other hand, our results for rapidly rotating models for PMS- and ZAMS-stars show emergence latitudes centered around 50° to 60°. Although larger magnetic fluxes, corresponding to the sizes of the observed spots, would shift the emergence somewhat towards the poles (cf. Sect. 5.2, Fig. 6), it seems clear that, in order to obtain polar spots in such stars, an additional mechanism acting upon the already emerged flux is required. Possibilities are a poleward meridional flow transporting magnetic flux at the surface (as observed in the case of the Sun) or the poleward slip of the submerged part of a flux tube dragging along with it the erupted part at the surface (Schüssler 1996). Indications for a poleward motion of mid-latitude spots on the RS CVn binary HR1099 have indeed been reported (Vogt et al. 1999, Strassmeier & Bartus 1999).

Simultaneous spot occurrence in extended latitudinal zones or in two separated latitudinal zones, mostly at or near the pole and at low-to-intermediate latitudes, is found in recent Doppler-imaging studies of young stars and also of main-sequence stars. Examples include the weak-line T-Tauri star V410 Tau (Strassmeier et al. 1994, Joncour et al. 1994b, Hatzes 1995a, Rice & Strassmeier 1996) as well as the T-Tauri stars Sz 68 (Johns-Krull & Hatzes 1997) and Par 1724 (e.g. Neuhäuser et al. 1998). On the other hand, low-latitude features are absent in the case of HDE 283572, a weak-line T Tauri star with a large polar spot (Joncour et al. 1994a, Strassmeier & Rice 1998b). A bimodal spot distribution, i.e. a polar spot and a number of low-latitude spots, were reported for the rapidly-rotating ZAMS star AB Dor (e.g. Kürster et al. 1994, Unruh et al. 1995). Similar distributions were found on the Pleiades-age MS-star LQ Hya (e.g. Rice & Strassmeier 1998, Donati 1999), on the rapidly-rotating α-Per-stars He699 and He520 (Barnes et al. 1998), and on the young G1.5V field star EK Dra (Strassmeier & Rice 1998a).

Our model so far can directly account for the simultaneous existence of polar and lower-latitude spots only in the case of rapidly-rotating T-Tauri stars with very small radiative cores. Here, axisymmetric instability leads to flux emergence near the poles while instability with $m \geq 1$ entails low-latitude eruption, so that a bimodal distribution results (cf. Fig. 4, top row). Depending on stellar mass, models for PMS stars after the T-Tauri phase and for stars on the ZAMS tend to have more or less extended unimodal latitude ranges of flux emergence, which shift poleward with increasing angular velocity. The existence or not of such a systematic relation between average emergence latitude and rotation would be an interesting observational test for our model. We suggest that the observed bimodal distributions on PMS and MS stars are due to a poleward transport of magnetic flux *after emergence* by meridional flow and/or magnetic stresses, thereby maintaining the polar magnetic features. The complex magnetic field structure with polarity changes indicated by the observations of Donati et al. (1997) are consistent with this interpretation.

The low-mass models with $\Omega \geq 4\ \Omega_\odot$ (cf. the 0.4-$M_\odot$ models in Fig. 4c) show spot emergence restricted to a narrow band at latitudes between ≈60–70°. Such a unique configuration should be detectable with modern Doppler-imaging techniques. Unfortunately, no Doppler images of such stars yet exist. The only M-dwarf stars mapped so far are the two M1Ve components of the close eclipsing binary YY Gem (Hatzes 1995b), but these stars have already evolved away from the ZAMS. Furthermore, imaging suffers from the north-south ambiguity due to the missing inclination of the stellar rotation axis with respect to the line of sight and also from severe spectral blending by molecular bands (Strassmeier 1999).

Further development of the theoretical model concerns mainly the evolution of a flux tube after its emergence, the influence of meridional flow and poleward slip as well as the interaction and possible reconnection of neighbouring flux tubes. It would also be promising to include information on stellar tachoclines from models of the angular momentum evolution of stars. This could give an indication whether the large critical field strengths necessary for instability in the case of rapid rotation (up to 10^7 G, cf. Fig. 2) can indeed be reached by shearing due to radial differential rotation or if further amplification through explosion or related processes (Moreno-Insertis et al. 1995) is required. With such large field strengths, a large amount of magnetic flux can be stored in a still very thin flux tube within the stellar overshoot layer.

In a recent paper, Donati (1999) claimed that the extended regions of azimuthal magnetic field resulting from his application of the Zeeman-Doppler imaging technique (Semel 1989) indicate the operation of a distributed dynamo in the stellar convection zone as opposed to an overshoot-layer dynamo. While it is well possible that some stellar dynamos operate fundamentally different from the solar dynamo, we consider Donati's conclusion as premature: a unipolar azimuthal field component also results in a natural way from a $m = 0$ instability, i.e., from an emerging toroidal flux tube. Alternatively, if a tube breaks into a number of bipolar magnetic regions in a sea-serpent fashion, these would also be connected by horizontal (azimuthal) field. Low-lying horizontal field is observed in sunspot penumbrae and 'canopies' (e.g., Solanki et al. 1994) and also in the weak intranetwork fields, but these fields are much more localized than the extended stretches of azimuthal field in the maps of Donati (1999). What is really puzzling in these observations is not so much the origin of the field (local, convection zone, or overshoot layer) but how such a large-scale horizontal field *in the stellar photosphere* is kept coherent against the action of convection, buoyancy and related instabilities.

On the other hand, the X-ray activity of fully convective low-mass stars (e.g. Fleming et al. 1995) and of chromospherically inactive stars (Saar 1998) indicates that some kind of distributed dynamo seems to operate in any star with an outer convection zone. It is questionable, however, whether such a 'turbulent' dynamo in the convection zone can give rise to starspots and large-scale coherent field patterns. In the case of the Sun, $\alpha\Omega$-models of distributed dynamo action based on the helioseismologically observed differential rotation fail to reproduce the basic properties of the solar cycle, like the butterfly diagram (e.g. Schmitt 1993), not to speak of the problem of flux storage (Moreno-Insertis et al. 1992).

7. Conclusions

Our results lend further support to the original suggestion by Schüssler & Solanki (1992) that the effect of the Coriolis force on rising flux tubes leads to high-latitude emergence of magnetic flux on rapidly rotating active stars.

Using simulations of unstable flux tubes rising through the convection zones of models of young stars covering significant ranges in mass, age, and angular velocity can predict latitudinal emergence patterns of starspots. We find extended latitude ranges of flux eruption and with simultaneous polar and low-latitude spots in the case of very young stars (presumably corresponding to the T-Tauri phase). Pre-main-sequence stars and zero-age-main-sequence stars show more or less broad unimodal ranges of emergence latitude, which shift equatorward with increasing stellar mass, decreasing angular velocity, and increasing age of the star. Such dependences possibly lend themselves to observational test. The formation of truly polar spots on such stars requires latitudinal transport of magnetic flux after its emergence at the surface.

Our detailed parameter study shows that the emergence latitudes are much more strongly influenced by variations of the flux-tube parameters (particularly initial location, field strength and magnetic flux) than by parameter variations affecting stellar structure. However, even drastic variations of the flux tube parameters do not alter our main results, the main effect being a broadening of the latitudinal emergence patterns. Further development of the model is expected mainly from the inclusion of realistic tachoclines and meridional flows, from improvements of the description of convective overshoot, and from attempts to simulate the evolution of magnetic flux after its emergence at the surface.

Acknowledgements. TG and KGS are very grateful to the Austrian Fond zur Förderung der wissenschaftlichen Forschung (FWF) for support under grant S7302-AST, and acknowledge the hospitality during various stays at the KIS.

References

Alexander D.R., Ferguson J.W., 1994, ApJ 437, 879
Barnes J.R., Collier Cameron A., Unruh Y. C., Donati J.-F., Hussain G.A.J., 1998, MNRAS 299, 904
Basu S., 1997, MNRAS 288, 572
Basu S., Antia H.M., 1997, MNRAS 287, 189
Bruls J.H.M.J., Solanki S.K., Schüssler M., 1998, A&A 336, 231
Buzasi D.L., 1997, ApJ 484, 855
Byrne P.B., 1996, in Strassmeier K.G., Linsky J.L. (eds.), IAU Symp. 176, Stellar Surface Structure, Kluwer Academic Press, Dordrecht, p. 299
Caligari P., Moreno-Insertis F., Schüssler M., 1995, ApJ 441, 886
Charbonneau P., Tomczyk S., Schou J., Thompson M.J., 1998, ApJ 496, 1015
Choudhuri A.R., D'Silva S., 1990, A&A 239, 326
Corbard T., Berthomieu G., Morel P., et al., 1997, A&A 324, 298
D'Antona F., Mazzitelli I., 1997, in Micela G., Pallavicini R., Sciortino S. (eds.), Cool Stars in Clusters and Associations, Mem.S.A.It. 68, p. 807
DeLuca E.E., Fan Y., Saar S.H., 1997, ApJ 481, 369
Donati J.-F., 1999, MNRAS 302, 457
Donati J.-F., Semel M., Carter B.D., Rees D.E., Cameron, A.C., 1997, MNRAS 291, 658
Fan Y., Fisher G., DeLuca E.E., 1993, ApJ 405, 390
Ferriz-Mas A., Schüssler M., 1993, Geophys. Astrophys. Fluid Dyn. 72, 209
Ferriz-Mas A., Schüssler M., 1995, Geophys. Astrophys. Fluid Dyn. 81, 233
Fleming T.A., Schmitt J.H.M.M., Giampapa M.S., 1995, ApJ 450, 401
Hall D.S., 1990, in Tuominen I., Moss D., Rüdiger G. (eds.), IAU Colloq. 130, The Sun and Cool Stars: Activity, Magnetism, Dynamos, Springer Verlag, Heidelberg, p. 353
Hatzes A.P., 1995a, ApJ 451, 784
Hatzes A.P., 1995b, in Strassmeier K.G. (ed.), Poster Proceedings IAU Symp. 176, Stellar Surface Structure, Univ. of Vienna, p. 90
Hatzes A.P., Vogt S.S., Ramseyer T.F., Misch A., 1996, ApJ 469, 808
Iglesias C.A., Rogers F.J., 1996, ApJ 464, 943
Johns-Krull C.M., 1996, A&A 306, 803
Johns-Krull C.M., Hatzes A.P., 1997, ApJ 487, 896
Joncour I., Bertout C., Bouvier J., 1994a, A&A 291, L19
Joncour I., Bertout C., Menard F., 1994b, A&A 285, L25
Kippenhahn R., Weigert A., Hofmeister E., 1967, Meth. Comp. Phy. 7, 129
Kitchatinov L.L., Rüdiger G., 1995, A&A 299, 446
Küker M., Rüdiger G., 1997, A&A 328, 253
Kürster M., Schmitt J.H.M.M., Cutispoto G., 1994, A&A 289, 899
Mihalas D., Hummer D.G., Mihalas B.W., Däppen W., 1990, ApJ 350, 300
Moreno-Insertis F., 1983, A&A 122, 241
Moreno-Insertis F., Schüssler M., Ferriz-Mas, A., 1992, A&A 264, 686
Moreno-Insertis F., Caligari P., Schüssler M., 1995, ApJ 452, 894
Neuhäuser R., Wolk S.J., Torres G., et al., 1998, A&A 334, 873
Rice J.B., Strassmeier K.G., 1996, A&A 316, 164
Rice J.B., Strassmeier K.G., 1998, A&A 336, 972
Rogers F.J., Iglesias C.A., 1992, ApJS 79, 507
Rogers F.J., Swenson F.J., Iglesias C.A., 1996, ApJ 456, 902
Saar S.H., 1998, in Donahue R., Bookbinder J. (eds.), Proc. 10^{th} Cambridge Workshop on Cool Stars, Stellar Systems, and the Sun, Cambridge, CD-1977
Schmitt D., 1993, in F. Krause, K.-H. Rädler, G. Rüdiger (eds.): The Cosmic Dynamo, IAU-Symposium 157, Kluwer, Dordrecht, p. 1
Schou J., Christensen-Dalsgaard J., Thompson M. J., 1994, ApJ 433, 389
Schüssler M., 1996, in Strassmeier K.G., Linsky J.L. (eds.), IAU Symp. 176, Stellar Surface Structure, Kluwer Academic Press, Dordrecht, p. 269

Schüssler M., Solanki S.K., 1992, A&A 264, L13
Schüssler M., Caligari P., Ferriz-Mas A., Solanki S.K., Stix M., 1996, A&A 314, 503 (Paper I)
Semel M., 1989, A&A 225, 456
Shaviv G., Salpeter E.E., 1973, ApJ 184, 191
Skaley D., Stix M., 1991, A&A 241, 227
Solanki S.K., Montavon C.A.P., Livingston W., 1994, A&A 283, 221
Strassmeier K.G., 1999, in Rebolo R. et al. (eds.), Euroconference on Very Low-Mass Stars and Brown Dwarfs, LaPalma, Cambridge Univ. Press, in press
Strassmeier K.G., Bartus J., 1999, A&A, submitted
Strassmeier K.G., Rice J.B., 1998a, A&A 330, 685
Strassmeier K.G., Rice J.B., 1998b, A&A 339, 497
Strassmeier K.G., Welty A.D., Rice J.B., 1994, A&A 285, L17
Tomczyck S., Schou J., Thompson M.J., 1995, ApJ 448, L57
Unruh Y.C., Collier Cameron A., 1997, MNRAS 290, L37
Unruh Y.C., Collier Cameron A., Cutispoto G., 1995, MNRAS 277, 1145
Vogt S.S., Penrod G.D., 1983, PASP 95, 565
Vogt S.S., Hatzes A.P., Misch A.A., Kürster M., 1999, ApJS, in press
Weiss A., Keady J.J., Magee Jr.N.H., 1990, Atomic Data Nucl. Data Tables 45, 209
Zwaan C., 1987, ARA&A 25, 83